

Unsupervised Learning Discriminative MIG Detectors in Nonhomogeneous Clutter

Xiaoqiang Hua, Yusuke Ono, Linyu Peng, *Member, IEEE*, and Yuting Xu

Abstract—Principal component analysis (PCA) is a commonly used pattern analysis method that maps high-dimensional data into a lower-dimensional space maximizing the data variance, that results in the promotion of separability of data. Inspired by the principle of PCA, a novel type of learning discriminative matrix information geometry (MIG) detectors in the unsupervised scenario are developed, and applied to signal detection in nonhomogeneous environments. Hermitian positive-definite (HPD) matrices can be used to model the sample data, while the clutter covariance matrix is estimated by the geometric mean of a set of secondary HPD matrices. We define a projection that maps the HPD matrices in a high-dimensional manifold to a low-dimensional and more discriminative one to increase the degree of separation of HPD matrices by maximizing the data variance. Learning a mapping can be formulated as a two-step mini-max optimization problem in Riemannian manifolds, which can be solved by the Riemannian gradient descent algorithm. Three discriminative MIG detectors are illustrated with respect to different geometric measures, i.e., the Log-Euclidean metric, the Jensen-Bregman LogDet divergence and the symmetrized Kullback-Leibler divergence. Simulation results show that performance improvements of the novel MIG detectors can be achieved compared with the conventional detectors and their state-of-the-art counterparts within nonhomogeneous environments.

Index Terms—Signal detection, matrix information geometry (MIG) detectors, unsupervised learning, manifold projection, nonhomogeneous clutter.

I. INTRODUCTION

IMPROVING the performance of signal detection in nonhomogeneous clutter is imperative in many areas, including radar [1]–[5], sonar [6]–[8], communication systems [9]. However, the detection performance is often unsatisfactory as the number of homogeneous sample data is often limited, not to mention the presence of interferences caused by the heterogeneity. One effective approach for enhancing the detection performance in nonhomogeneous clutter is to incorporate *a priori* clutter information in designing the detectors, i.e., carrying out a knowledge-aided processing (see, e.g., [10]–[12]), and performance analysis confirmed the advantage of such an architecture over their conventional counterparts (see

also [13]–[18]). That these knowledge-aided signal detection methods can achieve significant performance improvements is owing to the sufficient information on the clutter characteristics which is often not available priorly in practical applications. Lack of knowledge about the clutter can often yield severe performance degradation.

In recent years, exploiting matrix information geometry (MIG) to deal with the problem of signal processing has been attracting extensive attention. MIG, the geometric study of matrix manifolds, is a relative new extension of the theory of classical information geometry, which deals with the geometric theory of probability distributions and its applications [19]–[24]. The reader may refer to [25], [26] for an introduction to classical information geometry. Many information and signal processing problems can be equivalently transformed into discriminational problems on matrix differentiable manifolds with proper distance or divergence functions. For instance, in [27], an MIG-based clutter covariance matrix (CCM) estimator was proposed in the case of limited number of sample data, and significant signal-to-interference-plus-noise ratio gains were achieved over several standard estimators, such as the loaded sample matrix inversion. In [28], a new direction of arrival (DOA) estimation approach that employs geodesic distances to estimate the direction of arrival of several sources was proposed using the MIG theory. The DOA estimation was reformulated as a single-variable optimization problem on a Riemannian manifold. Simulation results showed that the proposed method improved resolution capabilities at low signal-to-noise ratio with respect to multiple signal classification and minimum variance distortionless response. In [29], the problem of CCM estimation was treated as computing the geometric barycenter associated with a geometric distance for a set of secondary basic Hermitian positive-definite (HPD) matrices that yielded significant performance improvements. Specially, a geometric detection scheme, which we call the MIG detector, was developed by Lapuyade-Lahorgue and Barbaresco in [30]. In MIG detectors, by taking geometric structures of the relevant manifolds into account, *a priori* knowledge on the clutter characteristics is not required.

The performance of MIG detectors is closely related to the discriminative power of the utilized geometric measures, e.g., [31], [32]. In particular for HPD manifolds, the affine invariant Riemannian metric (AIRM) and the corresponding AIRM-MIG detector have been greatly studied and applied [33]–[40]. By exploiting discriminative geometric measures, it is possible to propose MIG detectors of good performances. In [41], they authors derived the geometric means and medians corresponding to two extended Kullback–Leibler (KL) divergences,

This work was supported by NSFC (Grant No. 61901479), JSPS KAKENHI (Grant No. JP20K14365), JST CREST (Grant No. JPMJCR1914), and Keio Gijuku Fukuzawa Memorial Fund. We thank the editor and the anonymous referees for their constructive comments. (*Corresponding author: Linyu Peng.*)

X. Hua is with the College of Meteorology and Oceanography, and the College of Computer Science and Technology, National University of Defense Technology, Changsha 410073, China (e-mail: hxq712@yeah.net).

Y. Ono and L. Peng are with the Department of Mechanical Engineering, Keio University, Yokohama 223-8522, Japan (e-mail: yuu555yuu@keio.jp; l.peng@mech.keio.ac.jp).

Y. Xu is with the College of Physics, Jilin University, Changchun 130012, China (e-mail: xuyt20@mails.jlu.edu.cn).

the total KL divergence and the symmetrized KL divergence (SKLD), and particularly designed two MIG detectors based on the extended KL divergences. They were applied to target detection in K-distribution clutter, that evidenced performance gains over their state-of-the-art counterparts. In [42], [43], the total Bregman divergence (TBD) was extended to HPD matrix manifolds, and fortunately the geometric means derived by using the some of the mostly well-known convex functions could be derived in closed-form. Simulation results showed that the corresponding TBD-MIG detectors outperformed the AIRM-MIG detector as well as the conventional detectors in nonhomogeneous clutter. In addition to the discriminative geometric measures mentioned above, other measures can also be defined in HPD matrix manifolds. It is worth exploring new discriminative metrics and designing the corresponding MIG detectors. A major limitation in these MIG detectors, nevertheless, is that the detection performance is affected by different clutter characteristics as the discriminative power associated with a given geometric measure may change as the clutter changes.

To overcome the drawback, in this paper, we develop a projection that maps higher-order HPD matrices into a lower-dimensional and more discriminative HPD manifold and enhances the separability of data in the unsupervised learning scenario; then we propose a type of discriminative MIG detectors, and apply them to signal detection in nonhomogeneous clutter. Main contributions of the current study are briefly summarized below.

- 1) Inspired by the principle of principal component analysis (PCA), we propose a projection subject to an orthonormal constraint for the projection matrix, that enhances the separability between the target signal and the clutter. Learning the projection (matrix) by maximizing the variance of data becomes a two-step mini-max optimization problem in a Stiefel manifold and an HPD manifold, that can be solved by the Riemannian gradient descent (RGD) algorithm. Given a set of training HPD matrices that consists of two classes of data, one containing target signal and another containing only the clutter, the projection matrix can be obtained in an unsupervised way. One may consider that the PCA can only reconstruct the data in a better way but cannot lead to discrimination improvement between the samples. However, during the project, redundant information originally included in the higher-dimensional HPD matrices may be reduced during the manifold projection, leading to improvement of detection performance. From this aspect, the inspiration from PCA is rather indirect.
- 2) A class of discriminative MIG detectors is designed by incorporating the manifold projection into the detection architecture. Specifically, the sample data is modeled as an HPD matrix with the diagonal loading structure, and the CCM is estimated by the geometric mean about secondary HPD matrices. The CCM and the HPD matrix in the cell under test (CUT) are transformed into a more discriminative low-dimensional manifold. Consequently, signal detection is realized via MIG detector on a lower-

dimensional HPD matrix manifold.

- 3) Simulations performed in nonhomogeneous clutter verify the outperformance of the proposed discriminative MIG detectors in comparison with their state-of-the-art counterparts as well as the conventional detectors.

The paper is organized as follows. The discriminative MIG detector is formulated in Section II, and a brief introduction to MIG is given in Section III. In Section IV, three geometric means are derived for the CCM estimation, and the problem of learning the projection is formulated as a two-step mini-max optimization problem in a Stiefel manifold and an HPD manifold. The performance analysis is presented in Section V, and we conclude finally in Section VI.

Notations: We use boldface lowercase (uppercase) letters to denote vectors (matrices). Matrix (or vector) transpose and conjugate transpose are denoted by the superscripts $(\cdot)^T$ and $(\cdot)^H$, respectively. Determinant and trace of a matrix are respectively denoted by $\det(\cdot)$ and $\text{tr}(\cdot)$. The $N \times N$ identity matrix is denoted by \mathbf{I}_N or simply \mathbf{I} . The notations \mathbb{C}^N and $\mathbb{C}^{M \times N}$ represent the set of n -dimensional complex vectors and $M \times N$ complex matrices, respectively. The imaginary unit is i , and finally $\mathbb{E}[\cdot]$ denotes the statistical expectation.

II. PROBLEM FORMULATION

Let $\mathbf{x} = [x_0, x_1, \dots, x_{N-1}]^T$ be the sample data collected from N (temporal, spatial, or spatial-temporal) channels. In general, the problem of signal detection is interpreted as the following binary hypothesis testing

$$\begin{cases} \mathcal{H}_0 : \begin{cases} \mathbf{x} = \mathbf{c}, \\ \mathbf{x}_k = \mathbf{c}_k, \quad k \in [K], \end{cases} \\ \mathcal{H}_1 : \begin{cases} \mathbf{x} = \alpha \mathbf{p} + \mathbf{c}, \\ \mathbf{x}_k = \mathbf{c}_k, \quad k \in [K], \end{cases} \end{cases} \quad (1)$$

where $[K]$ denotes the set of $\{1, 2, \dots, K\}$ with K the number of secondary data, \mathbf{c} and \mathbf{c}_k are the clutter data, and \mathbf{x} and \mathbf{x}_k denote the observation data. In particular, \mathbf{x} and \mathbf{c} represent data of the CUT. Here, \mathcal{H}_0 and \mathcal{H}_1 denote the null and alternative hypotheses that correspond to the absence and presence of a target signal, respectively. The unknown complex parameter α is relevant to the channel propagation effects and target reflectivity. The known steering vector \mathbf{p} is given by

$$\mathbf{p} = \frac{1}{\sqrt{N}} [1, \exp(-i2\pi f_d), \dots, \exp(-i2\pi f_d(N-1))]^T, \quad (2)$$

where f_d denotes the normalized Doppler frequency.

The observation data is assumed to obey a multivariate complex Gaussian distribution with zero mean. Therefore, statistical information of the sample data is closely related to the covariance matrix. The power or correlation of the sample data, which can be represented as an HPD matrix, is employed for distinguishing the target signal from the clutter. Various structures can be specified for the HPD matrix, for instance, the Toeplitz structure [27], the diagonal loading [44], the shrinkage estimators [45] and the persymmetric covariance estimators [46]. The HPD manifolds subject to different matrix structures possess different geometric structures. The

resulting differences in the detection performance caused by different matrix structures will be analyzed separately. Here, we exploit the HPD matrix with the diagonal loading structure to model the sample data. The diagonal loading structure has been successfully applied in signal detection [47]–[49]. The diagonal loading HPD matrix can be expressed by adding diagonal matrix to the sample covariance matrix (SCM), i.e.,

$$\mathbf{R} = \mathbf{r}\mathbf{r}^H + \text{tr}(\mathbf{r}\mathbf{r}^H)\mathbf{I}, \quad (3)$$

where $\mathbf{r} = [r_0, r_1, \dots, r_{N-1}]^T$ denotes correlation of the sample data, namely

$$r_l = \mathbb{E}[x_i \bar{x}_{i+l}], \quad 0 \leq l \leq N-1, 1 \leq i \leq N-l-1. \quad (4)$$

where \bar{x}_i denotes the conjugate of x_i . Ergodicity of stationary Gaussian process allows us to approximate r_l by the following estimator

$$\tilde{r}_l = \frac{1}{N} \sum_{i=0}^{N-1-l} x_i \bar{x}_{i+l}, \quad 0 \leq l \leq N-1. \quad (5)$$

Using the diagonal loading formalism (3), each sample data can be represented as an HPD matrix with a diagonal loading structure as the new observation. The set of all $N \times N$ HPD matrices forms a differentiable manifold; see Section III for more details. Assuming that K secondary HPD matrices $\{\mathbf{R}_k\}_{k \in [K]}$ are available, we employ the geometric mean $\mathbf{R}_G = \mathcal{G}(\mathbf{R}_1, \mathbf{R}_2, \dots, \mathbf{R}_K)$ to estimate the CCM. From the viewpoint of MIG, the problem of binary hypothesis testing Eq. (1) can be rewritten as (see e.g., [43]),

$$\begin{cases} \mathcal{H}_0 : \mathbf{R} = \mathbf{R}_G, \\ \mathcal{H}_1 : \mathbf{R} \neq \mathbf{R}_G. \end{cases} \quad (6)$$

Given the observation \mathbf{R}_D and the CCM estimate \mathbf{R}_G , by utilizing geometric structure of HPD matrix manifolds, signal detection can be interpreted as the discrimination of two HPD matrices \mathbf{R}_D and \mathbf{R}_G in a differentiable manifold. Let us consider the null hypothesis $\mathcal{H}_0 : \mathbf{R} = \mathbf{R}_G$ versus the alternative hypothesis $\mathcal{H}_1 : \mathbf{R} \neq \mathbf{R}_G$ based on a set of observations $\{\mathbf{R}_k\}_{k \in [K]}$. The problem of signal detection can be understood as to determine the inner of isosurfaces of the HPD matrix manifold determined by a distance or divergence, as illustrated in Fig. 1. The hypothesis \mathcal{H}_0 is rejected if the observation \mathbf{R}_D of CUT does not belong to the inner of an isosurface.

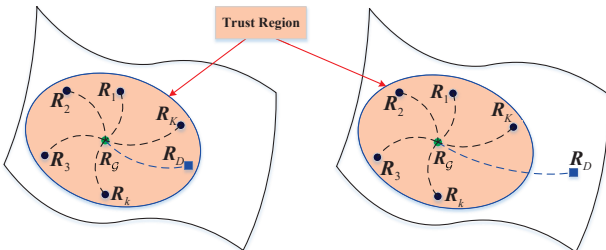


Fig. 1: The diagram for the geometric interpretation of signal detection

In our detection framework, we learn a projection matrix $\mathbf{W} \in \mathbb{C}^{N \times M}$ ($M \leq N$) of full rank to maximize the variance

of the data by resorting to the training HPD matrices in an unsupervised scenario, where any $N \times N$ HPD matrix \mathbf{R} will be mapped into a more discriminative low-dimensional manifold by

$$f_{\mathbf{W}}(\mathbf{R}) = \mathbf{W}^H \mathbf{R} \mathbf{W} \in \mathbb{C}^{M \times M}, \quad (7)$$

where \mathbf{W} is conventionally assumed in the (compact and complex) Stiefel manifold

$$\text{St}(M, \mathbb{C}^N) = \{\mathbf{A} \in \mathbb{C}^{N \times M} \mid \mathbf{A}^H \mathbf{A} = \mathbf{I}_M\}. \quad (8)$$

Consequently, the problem of signal detection becomes to determining the inner of an isosurface in an HPD matrix manifold associated to a given distance or divergence (see Fig. 1), namely

$$d(f_{\mathbf{W}}(\mathbf{R}_G), f_{\mathbf{W}}(\mathbf{R}_D)) \underset{\mathcal{H}_0}{\overset{\mathcal{H}_1}{\geq}} \gamma, \quad (9)$$

where $d(\cdot, \cdot)$ is the distance or divergence that used to measure the dissimilarity between two points on the HPD matrix manifold. The hypothesis \mathcal{H}_1 , meaning the presence of a target signal, is accepted if the observation $f_{\mathbf{W}}(\mathbf{R}_D)$ of CUT lies outside of an isosurface centered at $f_{\mathbf{W}}(\mathbf{R}_G)$ with radius γ , which is the detection threshold.

III. PRELIMINARIES OF MATRIX INFORMATION GEOMETRY

Before moving to an MIG solution to the problem formulated in Section II above, we briefly review the theory of MIG that is relevant to the current study in this section.

A. HPD manifolds

The general linear group $GL(N, \mathbb{F})$ consists of all $N \times N$ invertible matrices with \mathbb{F} either real \mathbb{R} or complex \mathbb{C} . The Frobenius metric¹ is defined by

$$\langle \mathbf{X}, \mathbf{Y} \rangle := \text{tr}(\mathbf{X}^H \mathbf{Y}), \quad \mathbf{X}, \mathbf{Y} \in GL(N, \mathbb{F}). \quad (10)$$

In the current paper, our main interest is HPD matrices, that form a subspace of $GL(N, \mathbb{C})$.

The set of $N \times N$ HPD matrices is denoted by $\mathcal{P}(N, \mathbb{C})$ which is a subset of $GL(N, \mathbb{C})$ and naturally a differentiable manifold. Each element $\mathbf{A} \in \mathcal{P}(N, \mathbb{C})$ is Hermitian and positive-definite, that is

$$\mathbf{A}^H = \mathbf{A} \text{ and } \mathbf{x}^H \mathbf{A} \mathbf{x} > 0 \text{ for all } \mathbf{0} \neq \mathbf{x} \in \mathbb{C}^N. \quad (11)$$

The difference of two HPD matrices can be evaluated by a distance, a divergence or other measures defined in $\mathcal{P}(N, \mathbb{C})$. It is crucial to specify these measures properly in applications, as different measures will lead to different isosurfaces.

¹It is also called the Hilbert–Schmidt inner product.

B. Riemannian structures of HPD manifolds

Except the induced subspace Frobenius metric, the space $\mathcal{P}(N, \mathbb{C})$ is a Riemannian manifold with the AIRM

$$\langle \mathbf{A}, \mathbf{B} \rangle_{\mathcal{P}} := \text{tr}(\mathbf{P}^{-1} \mathbf{A} \mathbf{P}^{-1} \mathbf{B}), \quad \mathbf{A}, \mathbf{B} \in T_{\mathcal{P}} \mathcal{P}(N, \mathbb{C}). \quad (12)$$

Under the AIRM, its curvature is non-positive [8], [50]–[52]. In the following, we are going to introduce some of the mostly well-known geometric measures in the manifold $\mathcal{P}(N, \mathbb{C})$ as either a metric space equipped with the Frobenius metric or a Riemannian manifold.

In the Riemannian manifold $\mathcal{P}(N, \mathbb{C})$, exponential map and logarithm map can naturally be defined on the tangent bundle $T_{\mathcal{P}} \mathcal{P}(N, \mathbb{C}) = \bigcup_{\mathbf{P}} T_{\mathbf{P}} \mathcal{P}(N, \mathbb{C})$ by using the geodesics. They are related to matrix exponentials and matrix logarithms. Matrix exponential for a general matrix \mathbf{X} is defined by a Taylor series

$$\exp(\mathbf{X}) = \sum_{i=0}^{+\infty} \frac{\mathbf{X}^i}{i!}. \quad (13)$$

Logarithm of a matrix is defined as the inversion of matrix exponential. Unfortunately, it is not always well-defined as a function. The following lemma defines the principle logarithm of an invertible matrix together with some of its important properties, which will be used later.

Lemma 1 ([53], [54]). *Let \mathbf{X} be an invertible matrix and assume that none of its eigenvalues lie in the closed negative real line. Then, there exists a unique matrix logarithm of \mathbf{X} whose eigenvalues lie in the strip*

$$\{z \in \mathbb{C} \mid -\pi < \text{Im}(z) < \pi\}.$$

It is referred to as the principle logarithm and denoted by $\text{Log } \mathbf{X}$.

The principle (matrix) logarithm satisfies the following properties.

- (i) Each pair of the matrices $[(\mathbf{X} - \mathbf{I})s + \mathbf{I}]^{-1}$, \mathbf{X} and $\text{Log } \mathbf{X}$ commutes any real number s .
- (ii) The following matrix integral is valid:

$$\begin{aligned} & \int_0^1 [(\mathbf{X} - \mathbf{I})s + \mathbf{I}]^{-2} ds \\ &= (\mathbf{I} - \mathbf{X})^{-1} [(\mathbf{X} - \mathbf{I})s + \mathbf{I}]^{-1} \Big|_{s=0}^1 \\ &= \mathbf{X}^{-1}. \end{aligned}$$

- (iii) Let $\mathbf{A}(\varepsilon)$ be an invertible matrix satisfying the unique principal logarithm existence condition above. Furthermore, assume $\mathbf{A}(\varepsilon)$ depends on the real parameter ε smoothly. Then we have

$$\begin{aligned} \frac{d}{d\varepsilon} \text{Log } \mathbf{A}(\varepsilon) &= \int_0^1 [(\mathbf{A}(\varepsilon) - \mathbf{I})s + \mathbf{I}]^{-1} \frac{d}{d\varepsilon} \mathbf{A}(\varepsilon) \\ &\quad \times [(\mathbf{A}(\varepsilon) - \mathbf{I})s + \mathbf{I}]^{-1} ds. \end{aligned}$$

In the Riemannian manifold $\mathcal{P}(N, \mathbb{C})$ equipped with the AIRM, the distance of two points $\mathbf{X}, \mathbf{Y} \in \mathcal{P}(N, \mathbb{C})$ is given

by the length of the local geodesic with them as the endpoints, reading

$$\begin{aligned} d_{\mathcal{R}}^2(\mathbf{X}, \mathbf{Y}) &= \left\| \text{Log} \left(\mathbf{X}^{-1/2} \mathbf{Y} \mathbf{X}^{-1/2} \right) \right\|^2 \\ &= \sum_{i=1}^N \ln^2 \lambda_i, \end{aligned} \quad (14)$$

where $\lambda_1, \lambda_2, \dots, \lambda_N$ are the eigenvalues of the matrix $\mathbf{X}^{-1/2} \mathbf{Y} \mathbf{X}^{-1/2}$. We use $\|\cdot\|$ to denote the Frobenius norm $\|\mathbf{A}\|^2 = \text{tr}(\mathbf{A}^H \mathbf{A})$ of a matrix \mathbf{A} , induced from the Frobenius metric (10).

Unfortunately, the computational cost of the AIRM distance is often expensive in practical applications. An alternative choice, the Log-Euclidean metric (LEM) [55], is defined as follows

$$\langle \mathbf{A}, \mathbf{B} \rangle_{\mathcal{P}}^{\text{LE}} := \langle D_{\mathbf{A}} \text{Log } \mathbf{P}, D_{\mathbf{B}} \text{Log } \mathbf{P} \rangle, \quad (15)$$

where $\mathbf{A}, \mathbf{B} \in T_{\mathcal{P}} \mathcal{P}(N, \mathbb{C})$ and $D_{\mathbf{A}} \text{Log } \mathbf{P}$ denotes the directional derivative of the matrix logarithm along a tangent vector \mathbf{A} at a point \mathbf{P} . The LEM distance of two HPD matrices $\mathbf{X}, \mathbf{Y} \in \mathcal{P}(N, \mathbb{C})$ is given by the length of the local geodesic as

$$d_{\mathcal{L}}^2(\mathbf{X}, \mathbf{Y}) = \|\text{Log } \mathbf{X} - \text{Log } \mathbf{Y}\|^2. \quad (16)$$

C. Divergences of HPD matrices

By viewing the differentiable manifold $\mathcal{P}(N, \mathbb{C})$ as a metric space equipped with the Frobenius metric, many other geometric measures can also be defined. We will be focused on the the Jensen–Bregman LogDet divergence (JBLD) [56] and the symmetrized Kullback–Leibler divergence (SKLD) [41] in the current paper. The JBLD and SKLD of two HPD matrices $\mathbf{X}, \mathbf{Y} \in \mathcal{P}(N, \mathbb{C})$ are respectively given by

$$d_{\mathcal{J}}^2(\mathbf{X}, \mathbf{Y}) = \ln \det \left(\frac{\mathbf{X} + \mathbf{Y}}{2} \right) - \frac{1}{2} \ln \det(\mathbf{X} \mathbf{Y}) \quad (17)$$

and

$$d_{\mathcal{S}}^2(\mathbf{X}, \mathbf{Y}) = \frac{1}{2} \text{tr}(\mathbf{Y}^{-1} \mathbf{X} + \mathbf{X}^{-1} \mathbf{Y} - 2\mathbf{I}). \quad (18)$$

Note that among all geometric measures introduced above, the AIRM, the JBLD and the SKLD are invariant with respect to affine transformations.

In the study of optimization problems in $\mathcal{P}(N, \mathbb{C})$, we often need to compute the gradient of a function $F(\mathbf{R})$, which is defined by the covariant/directional derivative associated to a given metric, e.g., a Riemannian metric or simply the Frobenius metric, as follows

$$\langle \nabla F(\mathbf{R}), \mathbf{A} \rangle := \frac{d}{d\varepsilon} \Big|_{\varepsilon=0} F(\gamma(\varepsilon)), \quad \forall \mathbf{A} \in T_{\mathbf{R}} \mathcal{P}(N, \mathbb{C}), \quad (19)$$

where $\gamma : [0, 1] \rightarrow \mathcal{P}(N, \mathbb{C})$ is the unique local curve satisfying $\gamma(0) = \mathbf{R}$ and $\dot{\gamma}(0) = \mathbf{A}$. By taking the linear part into account, it can be rewritten as

$$\langle \nabla F(\mathbf{R}), \mathbf{A} \rangle := \frac{d}{d\varepsilon} \Big|_{\varepsilon=0} F(\mathbf{R} + \varepsilon \mathbf{A}), \quad \forall \mathbf{A} \in T_{\mathbf{R}} \mathcal{P}(N, \mathbb{C}). \quad (20)$$

IV. GEOMETRIC MEANS AND UNSUPERVISED MANIFOLD PROJECTION

A. Geometric Means

It is well known that the arithmetic mean of a set of K positive real numbers $\{x_k\}_{k \in [K]}$ can be calculated by

$$\hat{x} = \frac{1}{K} \sum_{k=1}^K x_k. \quad (21)$$

In fact, the arithmetic mean is the minimum value of the sum of the squares, namely

$$\hat{x} := \arg \min_{x \in \mathbb{R}^+} \sum_{k=1}^K |x - x_k|^2, \quad (22)$$

where $|x - x_k|$ denotes the distance between x and x_k . Geometric mean of a set of HPD matrices can similarly be defined.

Definition 2. Given a set of K HPD matrices $\{\mathbf{R}_k\}_{k \in [K]}$, the geometric mean with respect to a geometric measure $d : \mathcal{P}(N, \mathbb{C}) \times \mathcal{P}(N, \mathbb{C}) \rightarrow \mathbb{R}$ is obtained through the following optimization problem

$$\hat{\mathbf{R}} := \arg \min_{\mathbf{R} \in \mathcal{P}(N, \mathbb{C})} \sum_{k=1}^K d^2(\mathbf{R}_k, \mathbf{R}). \quad (23)$$

Geometric means of a set of HPD matrices can not always be calculated in closed form; alternatively, the fixed-point iteration has proven to be effective for calculating them numerically, e.g., [31], [55], [57]. In the below, we summarize the algorithms or analytic expressions for computing the geometric means corresponding to the three measures introduced above, i.e., the LEM distance (16), the AIRM geodesic distance (14), the JBLD (17) and the SKLD (18).

Proposition 3. The LEM mean of HPD matrices $\{\mathbf{R}_k\}_{k \in [K]}$ is given by [55]

$$\hat{\mathbf{R}} = \exp\left(\frac{1}{K} \sum_{k=1}^K \text{Log } \mathbf{R}_k\right). \quad (24)$$

Proposition 4. The AIRM mean of $\{\mathbf{R}_k\}_{k \in [K]}$ is determined by [54]

$$\sum_{k=1}^K \text{Log}\left(\mathbf{R}_k^{-1} \hat{\mathbf{R}}\right) = 0, \quad (25)$$

which can be obtained using the following fixed-point iteration [58]:

$$\begin{aligned} \hat{\mathbf{R}}_{t+1} &= a \hat{\mathbf{R}}_t \\ &+ (a-1) \sum_{k=2}^K \text{Log}\left(\exp\left(\frac{\hat{\mathbf{R}}_t}{2}\right) \mathbf{R}_k^{-1} \exp\left(\frac{\hat{\mathbf{R}}_t}{2}\right)\right), \end{aligned} \quad (26)$$

where $1 - 1/K < a < 1$, t denotes the iterative index, and the initial value is

$$\hat{\mathbf{R}}_0 = \frac{1}{K} \sum_{k=1}^K \text{Log } \mathbf{R}_k. \quad (27)$$

Proposition 5. The JBLD mean of HPD matrices $\{\mathbf{R}_k\}_{k \in [K]}$ can be obtained through the fixed-point iteration [31], [57]:

$$\hat{\mathbf{R}}_{t+1} = \left(\frac{1}{K} \sum_{k=1}^K \left(\frac{\hat{\mathbf{R}}_t + \mathbf{R}_k}{2}\right)^{-1}\right)^{-1}. \quad (28)$$

Proposition 6. The SKLD mean of HPD matrices $\{\mathbf{R}_k\}_{k \in [K]}$ is

$$\hat{\mathbf{R}} = \mathbf{A}^{-1/2} \left(\mathbf{A}^{1/2} \mathbf{B} \mathbf{A}^{1/2}\right)^{1/2} \mathbf{A}^{-1/2}, \quad (29)$$

where

$$\mathbf{A} = \sum_{k=1}^K \mathbf{R}_k^{-1}, \quad \mathbf{B} = \sum_{k=1}^K \mathbf{R}_k. \quad (30)$$

Proof. A proof is provided in Appendix A; see also [59]. \square

B. Unsupervised Manifold Projection

In this subsection, we introduce the manifold projection that maps HPD matrices from a high-dimensional manifold to a more discriminative lower-dimensional one by maximizing the variance of data.

Recall that the variance of a set of vectors $\{\mathbf{x}_k\}_{k \in [K]}$ in a Euclidean space is given by

$$\text{Var} = \frac{1}{K} \sum_{k=1}^K \|\mathbf{x}_k - \hat{\mathbf{x}}\|_2^2 \quad \text{with} \quad \hat{\mathbf{x}} = \frac{1}{K} \sum_{k=1}^K \mathbf{x}_k, \quad (31)$$

where $\|\cdot\|_2$ denotes the l_2 norm, and $\hat{\mathbf{x}}$ is the mean of the set of vectors.

Given a set of HPD matrices $\{\mathbf{R}_i\}_{i \in [J+K]}$ that contains J CCMs and K HPD matrices with a target signal, the variance can similarly be defined as

$$\text{Var} = \frac{1}{J+K} \sum_{i=1}^{J+K} d^2\left(\mathbf{R}_i, \hat{\mathbf{R}}\right). \quad (32)$$

where $\hat{\mathbf{R}}$ denotes the mean of $J+K$ HPD matrices, which can be derived using Eq. (23) with respect to the LEM distance, the JBLD or the SKLD. Note that the variance (32) can be interpreted as a deterministic counterpart of the variance function of a probability distribution defined in the HPD manifold [60].

As briefly introduced in Section II, we propose a manifold projection that maps HPD matrices into a more lower-dimensional manifold maximizing the data variance. The projection is defined as

$$\begin{aligned} f_{\mathbf{W}} &: \mathcal{P}(N, \mathbb{C}) \rightarrow \mathcal{P}(M, \mathbb{C}) \\ \mathbf{R} &\mapsto \mathbf{W}^H \mathbf{R} \mathbf{W}, \end{aligned} \quad (33)$$

where $M \leq N$ and $\mathbf{W} \in \text{St}(M, \mathbb{C}^N) \subset \mathbb{C}^{N \times M}$. Obviously, \mathbf{W} is of maximal rank and $\mathbf{W}^H \mathbf{W} = \mathbf{I}_M$. Therefore, for a set of HPD matrices $\{\mathbf{R}_i\}_{i \in [J+K]}$ in $\mathcal{P}(N, \mathbb{C})$, learning a mapping to achieve maximal variance is equivalent to searching a projection matrix \mathbf{W} in the Stiefel manifold. Namely, the problem becomes solving the optimization problem

$$\begin{aligned} \overline{\mathbf{W}} &:= \arg \max_{\mathbf{W} \in \text{St}(M, \mathbb{C}^N)} \frac{1}{J+K} \sum_{i=1}^{J+K} d^2\left(f_{\mathbf{W}}(\mathbf{R}_i), \hat{\mathbf{Z}}\right) \\ &= \arg \max_{\mathbf{W} \in \text{St}(M, \mathbb{C}^N)} \frac{1}{J+K} \sum_{i=1}^{J+K} d^2\left(\mathbf{W}^H \mathbf{R}_i \mathbf{W}, \hat{\mathbf{Z}}\right), \end{aligned} \quad (34)$$

where $\widehat{\mathbf{Z}}$ is the geometric mean of the set $\{\mathbf{W}^H \mathbf{R}_i \mathbf{W}\}_{i \in [J+K]}$ in $\mathcal{P}(M, \mathbb{C})$, namely

$$\widehat{\mathbf{Z}} = \arg \min_{\mathbf{Z} \in \mathcal{P}(M, \mathbb{C})} \sum_{i=1}^{J+K} d^2(\mathbf{W}^H \mathbf{R}_i \mathbf{W}, \mathbf{Z}). \quad (35)$$

Remark 7. Solving the optimization problem (34) is a very complex and nonlinear problem as $\widehat{\mathbf{Z}} \in \mathcal{P}(M, \mathbb{C})$ also depends on \mathbf{W} . Although for the LEM distance and the SKLD, we can obtain the means (see Propositions 3 and 6) respectively as

$$\widehat{\mathbf{Z}}_L = \exp\left(\frac{1}{J+K} \sum_{i=1}^{J+K} \text{Log}(\mathbf{W}^H \mathbf{R}_i \mathbf{W})\right) \quad (36)$$

and

$$\widehat{\mathbf{Z}}_S = \mathbf{A}^{-1/2} \left(\mathbf{A}^{1/2} \mathbf{B} \mathbf{A}^{1/2}\right)^{1/2} \mathbf{A}^{-1/2}, \quad (37)$$

where

$$\mathbf{A} = \sum_{i=1}^{J+K} (\mathbf{W}^H \mathbf{R}_i \mathbf{W})^{-1}, \quad \mathbf{B} = \sum_{i=1}^{J+K} \mathbf{W}^H \mathbf{R}_i \mathbf{W}. \quad (38)$$

Since it is difficult to solve the projection matrix $\overline{\mathbf{W}}$ from (34) in closed-form, we formulate it as a two-step mini-max optimization problem as follows:

$$\begin{aligned} \overline{\mathbf{W}}_{t+1} &= \arg \max_{\mathbf{W} \in \text{St}(M, \mathbb{C}^N)} \frac{1}{J+K} \sum_{i=1}^{J+K} d^2(\mathbf{W}^H \mathbf{R}_i \mathbf{W}, \widehat{\mathbf{Z}}_t), \\ \widehat{\mathbf{Z}}_{t+1} &= \arg \min_{\mathbf{Z} \in \mathcal{P}(M, \mathbb{C})} \sum_{i=1}^{J+K} d^2(\overline{\mathbf{W}}_{t+1}^H \mathbf{R}_i \overline{\mathbf{W}}_{t+1}, \mathbf{Z}), \end{aligned} \quad (39)$$

where t denotes the iterative step. At each step, the minimal problem for $\widehat{\mathbf{Z}}$ can either be solved analytically by Remark 7 or numerically by Proposition 5; the maximal problem can be transformed into a minimal problem

$$\arg \min_{\mathbf{W} \in \text{St}(M, \mathbb{C}^N)} \psi(\mathbf{W}), \quad (40)$$

that can be solved by the RGD algorithm (44) (see also [61], [62]), where at each step t ,

$$\psi(\mathbf{W}) = -\frac{1}{J+K} \sum_{i=1}^{J+K} d^2(\mathbf{W}^H \mathbf{R}_i \mathbf{W}, \widehat{\mathbf{Z}}_t). \quad (41)$$

The Riemannian gradient of a function $\psi(\mathbf{W})$ defined on the Stiefel manifold $\text{St}(M, \mathbb{C}^N)$ is given by [63]

$$\text{grad } \psi(\mathbf{W}) = \nabla \psi(\mathbf{W}) - \mathbf{W} \times \text{sym}(\mathbf{W}^H \nabla \psi(\mathbf{W})), \quad (42)$$

where

$$\text{sym}(\mathbf{A}) = \frac{\mathbf{A} + \mathbf{A}^H}{2} \quad (43)$$

denotes the symmetric part of a matrix \mathbf{A} , and $\nabla \psi(\mathbf{W})$ is the Euclidean gradient induced from the Frobenius metric. The RGD algorithm reads

$$\mathbf{W}_{l+1} = \exp_{\mathbf{W}_l}(-\eta_l \text{grad } \psi(\mathbf{W}_l)), \quad (44)$$

where η_l is the step size, and $\exp : T\text{St}(M, \mathbb{C}^N) \rightarrow \text{St}(M, \mathbb{C}^N)$ is the exponential map associated to the Euclidean

metric of the Stiefel manifold. For more details, the reader may refer to [59], [63].

To compile the RGD algorithm (44), the Euclidean gradient of the function $\psi(\mathbf{W})$ is needed. Note that the Frobenius metric (10) can be extended to $N \times M$ matrices, namely

$$\langle \mathbf{X}, \mathbf{Y} \rangle = \text{tr}(\mathbf{X}^H \mathbf{Y}), \quad \mathbf{X}, \mathbf{Y} \in \mathbb{C}^{N \times M}. \quad (45)$$

Proposition 8. The Euclidean gradient of the function $\psi(\mathbf{W})$ defined by (41) associated with the LEM is given by

$$\begin{aligned} \nabla \psi(\mathbf{W}) &= -\frac{4}{J+K} \sum_{i=1}^{J+K} \mathbf{R}_i \mathbf{W} \left(\mathbf{V}^{-1} \text{Log } \mathbf{V} \right. \\ &\quad \left. - \int_0^1 [(\mathbf{V} - \mathbf{I})s + \mathbf{I}]^{-1} (\text{Log } \widehat{\mathbf{Z}}_t) \right. \\ &\quad \left. \times [(\mathbf{V} - \mathbf{I})s + \mathbf{I}]^{-1} ds \right), \end{aligned} \quad (46)$$

where $\mathbf{V} = \mathbf{W}^H \mathbf{R}_i \mathbf{W}$.

Proof. See Appendix B. \square

Proposition 9. The Euclidean gradient of the function $\psi(\mathbf{W})$ with respect to the AIRM is given by

$$\begin{aligned} \nabla \psi(\mathbf{W}) &= \frac{4}{J+K} \sum_{i=1}^{J+K} \mathbf{R}_i \mathbf{W} (\mathbf{W}^H \mathbf{R}_i \mathbf{W})^{-1} \\ &\quad \times \text{Log}(\widehat{\mathbf{Z}}_t (\mathbf{W}^H \mathbf{R}_i \mathbf{W})^{-1}). \end{aligned} \quad (47)$$

Proof. The corresponding function $\psi(\mathbf{W})$ is

$$\psi(\mathbf{W}) = -\frac{1}{J+K} \sum_{i=1}^{J+K} \text{tr} \left(\text{Log}^2 \left((\mathbf{W}^H \mathbf{R}_i \mathbf{W})^{-1} \widehat{\mathbf{Z}}_t \right) \right). \quad (48)$$

Using definition of the Euclidean gradient and following a similar proof of Appendix B, the result can be directly obtained. Similar computation details are omitted here. \square

Proposition 10. The Euclidean gradient of $\psi(\mathbf{W})$ associated with the JBLD is given by

$$\begin{aligned} \nabla \psi(\mathbf{W}) &= -\frac{1}{J+K} \sum_{i=1}^{J+K} \mathbf{R}_i \mathbf{W} \left(2 \left(\mathbf{W}^H \mathbf{R}_i \mathbf{W} + \widehat{\mathbf{Z}}_t \right)^{-1} \right. \\ &\quad \left. - \left(\mathbf{W}^H \mathbf{R}_i \mathbf{W} \right)^{-1} \right). \end{aligned} \quad (49)$$

Proof. See Appendix C. \square

Proposition 11. The Euclidean gradient of $\psi(\mathbf{W})$ associated with the SKLD is given by

$$\begin{aligned} \nabla \psi(\mathbf{W}) &= -\frac{1}{J+K} \sum_{i=1}^{J+K} \mathbf{R}_i \mathbf{W} \left(\widehat{\mathbf{Z}}_t^{-1} \right. \\ &\quad \left. - \left(\mathbf{W}^H \mathbf{R}_i \mathbf{W} \right)^{-1} \widehat{\mathbf{Z}}_t \left(\mathbf{W}^H \mathbf{R}_i \mathbf{W} \right)^{-1} \right). \end{aligned} \quad (50)$$

Proof. See Appendix D. \square

C. Complexity Analysis

In this subsection, we will briefly show the complexity of the calculation of LEM, AIRM, JBLD, SKLD means given by Propositions 3, 4, 5, 6 and the arithmetic mean, as well as the Euclidean gradients of $\psi(\mathbf{W})$ with respect to the LEM, AIRM, JBLD, SKLD, respectively. The latter are given by Propositions 8, 9, 10, 11. For simplicity, we only keep the leading terms; for numerical iterations, we only provide the computational complexity for a single step.

The complexity figures assume that K number of $N \times N$ HPD matrices are given and the arithmetic with individual elements has complexity $O(1)$. The lower HPD manifold is M -dimensional. The following facts are used: $\mathbf{R}^{-1} \sim O(N^3)$ and $\text{Log } \mathbf{R} \sim O(N^4)$. Matrix exponential in all algorithms only deal with Hermitian matrices, and one way to calculate their exponentials is through eigenvalue decomposition, whose complexity is $O(N^3)$, same as that of matrix inversion.

TABLE I: Computational complexity of the means

Geometric measures	Complexity
Arithmetic mean	$O(N^2(K-1))$
LEM (Proposition 3)	$O(N^4K)$
AIRM (Proposition 4, per iteration)	$O(N^4(K-1))$
JBLD (Proposition 5, per iteration)	$O(N^3(K+1))$
SKLD (Proposition 6)	$O(N^3(K+6))$

It is clear from TABLE I that the arithmetic mean costs least time, followed by the SKLD mean. Although both of them are Riemannian distances, computation of the LEM mean is much faster than the AIRM mean.

TABLE II: Computational complexity of the Euclidean gradients

Geometric measures	Complexity for each step (mod $J+K$)
LEM (Proposition 8)	$O(2M^4) + O(N^2M)$
AIRM (Proposition 9)	$O(M^4) + O(2N^2M)$
JBLD (Proposition 10)	$O(2M^3) + O(2NM^2) + O(2N^2M)$
SKLD (Proposition 11)	$O(4M^3) + O(2NM^2) + O(2N^2M)$

From TABLE II, we notice that computation of gradients of the divergences, i.e., the JBLD and the SKLD, costs less time compared with the Riemannian distances, i.e., the LEM and the AIRM. Main reason is again the latter depend on matrix logarithm.

V. SIMULATION RESULTS

In this section, we perform simulations to verify the performance advantage of the detectors proposed in the current paper, which are compared with the state-of-the-art counterparts.

A. Environment Setup

The simulations are performed in a non-homogeneous clutter, specifically, in a Gaussian clutter in the presence of interferences. We generate the sample data by resorting to an N -dimensional complex circular Gaussian distribution with zero mean and the known covariance matrix

$$\mathbf{C} = \sigma_c^2 \mathbf{C}_0 + \sigma_n^2 \mathbf{I}, \quad (51)$$

where $\sigma_c^2 \mathbf{C}_0$ denotes the clutter with σ_c^2 the clutter power while $\sigma_n^2 \mathbf{I}$ is the thermal noise with σ_n the noise power. Therefore, the clutter-to-noise ratio (CNR) is given by

$$\text{CNR} = \frac{\sigma_c^2}{\sigma_n^2}. \quad (52)$$

The structure of the CCM \mathbf{C}_0 is Gaussian shaped with one-lag correlation coefficient ρ , whose entries are given by

$$[\mathbf{C}_0]_{i,j} = \rho^{|i-j|} \exp(i 2\pi f_c (i-j)), \quad i, j = 1, 2, \dots, N. \quad (53)$$

Here, f_c is the normalized Doppler frequency. K secondary HPD matrices derived from the diagonal loading formalism (3) are employed to estimate the CCM matrix as \mathbf{R}_G . The HPD matrix \mathbf{R}_D in the CUT is computed by the sample data \mathbf{x}_D . In the following, the parameters are chosen as $\sigma_n^2 = 1$, CNR = 25 dB, $\rho = 0.95$ and $f_c = 0.1$.

B. The Training Data

The dimension of the sample data is set to be $N = 8$. The normalized Doppler frequency of target signal is set to $f_s = 0.2$. Two interferences are injected into the secondary data with the normalized Doppler frequency $f = 0.22$. The training dataset consists of two subsets with the size of 2000 each: the set of CCM and the set of HPD matrices containing a signal with SCR = 25 dB. Fig. 2 shows the distance between the CCMs and the HPD matrices with a target signal for different measures. In particular, within the cases of AIRM, LEM and JBLD, the clutter-clutter distances are more scattered compared with the clutter-target distances, while conversely the clutter-target distances are more scattered under the SKLD.

C. Comparison with Relevant Algorithms

In order to verify the effectiveness of the proposed detectors, we compare the proposed methods with several well-received algorithms. For convenience, the following abbreviations are adopted.

- AMF: The traditional adaptive matched filter [64].
- Benchmark: The AMF with known covariance matrix. It is the optimal performance for the types of AMFs.
- TBD-MIG detectors: The MIG detectors with the total square loss (TSL), the total von-Neumann (TVN) divergence, and the total log-determinant (TLD) divergence [42], [43].

Unlike the AMF, the optimal performance of MIG detectors is not the MIG detectors with the known CCM since the detection performance is closely related to the discrimination between the target signal and the clutter. To decrease the computational load, we choose the probability of false alarm as $P_{fa} = 10^{-3}$. A number of $100/P_{fa}$ independent trials are repeated to estimate the threshold, while 2000 independent trials are repeated to estimate the probability of detection P_d .

D. Simulation Results and Discussions

By using the training dataset, we derive the three projection matrices that transforms the $N \times N$ HPD matrices to $M \times M$

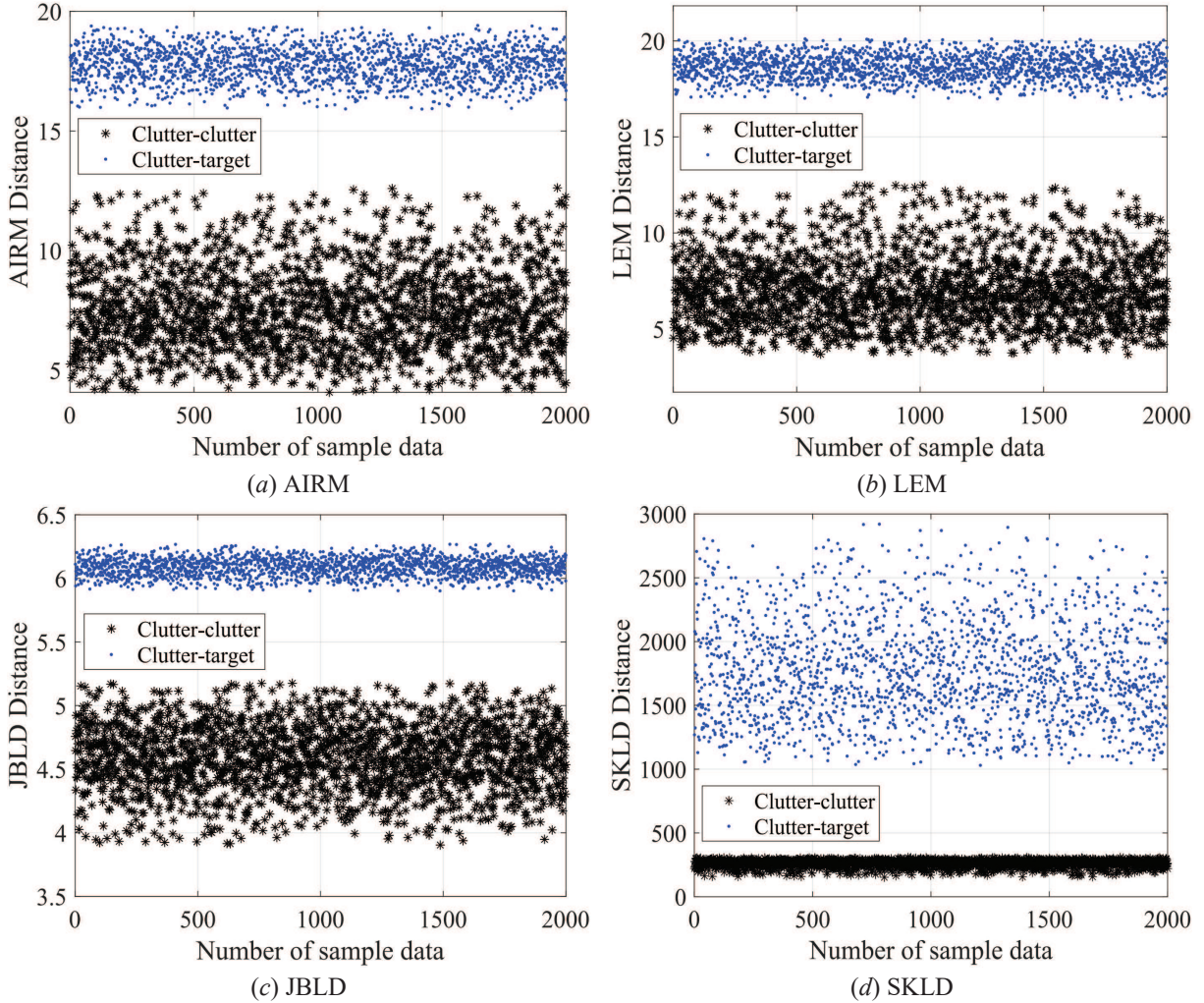


Fig. 2: Clutter-target distance for different measures

HPD matrices for $M = 8, 6, 4,$ and $2,$ respectively. We then perform the signal detection on these manifolds for different size of K secondary data, where $K = M, 1.5M,$ and $2M,$ respectively. Statistically, as K increases, the estimate accuracy of the CCM improves, that will certainly affect the detection performance. Figs. 3, 4 and 5 plot the P_d vs SCR for the proposed MIG detectors and their corresponding counterparts as well as the TBD-MIG detectors and the AMF under different sizes of secondary data. The AMF with the known CCM is also provided as a benchmark. Figs. 3, 4 and 5 show that the detection performances of all the considered detectors improve as K becomes larger. In Fig. 3, the MIG detectors can still work well while the P_d of the AMF is very low, because that the estimate accuracy of the SCM is worse when $K = M$. It should also be noticed that all the MIG detectors with manifold projection have better performances compared with their unprojected counterparts, namely the original MIG detectors, and both the projected and unprojected MIG detectors outperform the AMF except for the SKLD-MIG detector under $K = 2M$. In other words, the manifold projection can promote the discriminative power of HPD matrices. Moreover, the TBD-MIG detectors outperform

the unprojected AIRM and LEM MIG detectors and both the projected and unprojected SKLD MIG detectors.

To analyze the difference in the detection performance for different measure-based MIG detectors. Fig. 6 shows the results of P_d vs SCRs for different measures. It is obvious that the JBLD MIG detector has the best performance. Detection performance of the AIRM, LEM, and TBD is similar and they are better than the SKLD when $K > M$. It should be noted that it is probably difficult to determine detector which is universally better compared with the others since performance of the detection methods can also depend on features of the clutter. One important future research would be determining the best detector against a specific type of clutter.

VI. CONCLUSIONS

In this paper, we proposed a class of learning discriminative MIG detectors in the unsupervised scenario, and applied them for signal detection in nonhomogeneous clutter. The sample data was interpreted as an HPD matrix, and the secondary HPD matrices were used to estimate the CCM. Inspired by the principle of PCA, we constructed a manifold projection that maps higher-order HPD matrices to a more discriminative

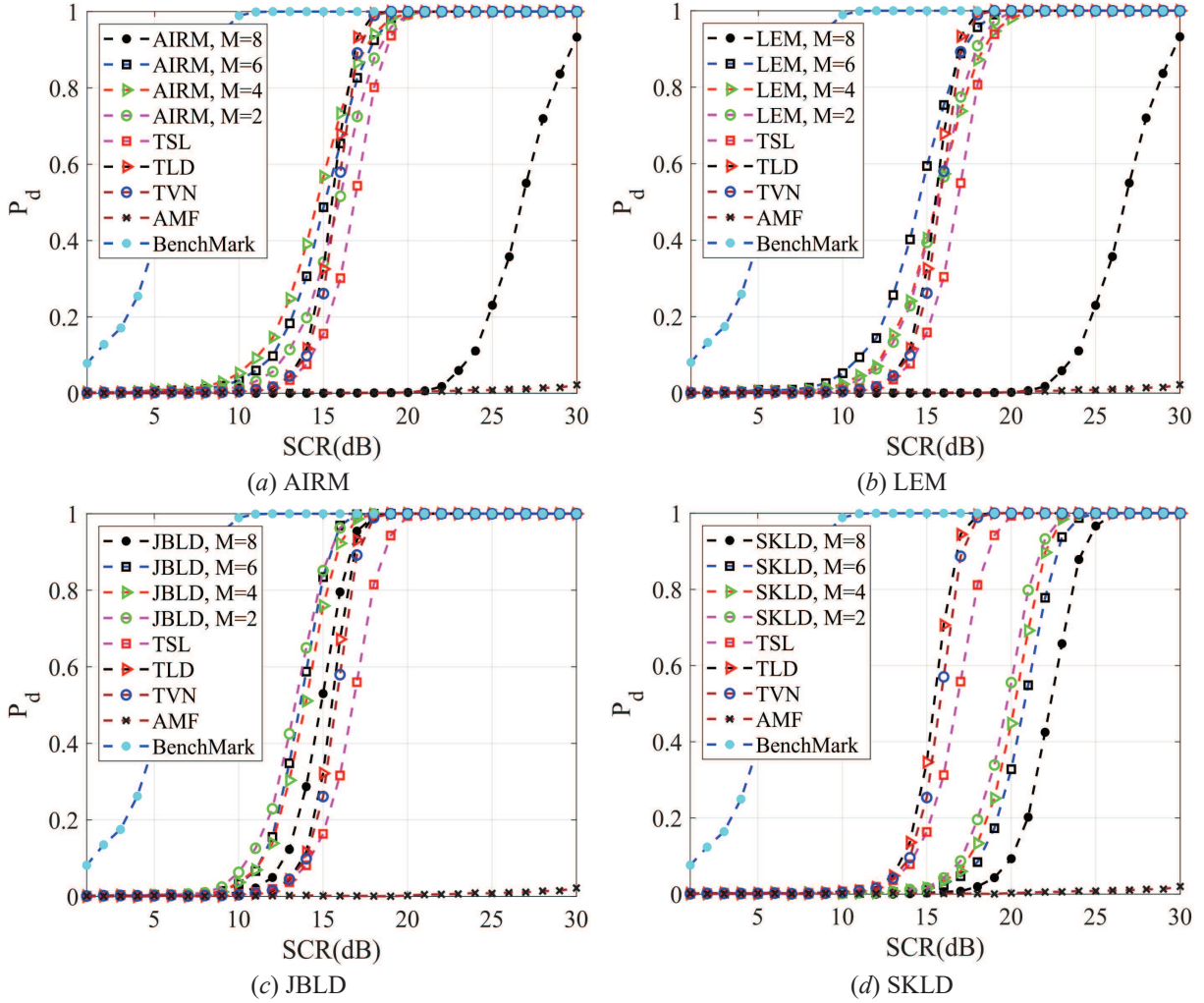


Fig. 3: The plots of P_d vs SCR for $K = M$ in the nonhomogeneous clutter with two interferences.

lower-dimensional HPD manifold with maximum data variance. Learning the projection with maximum data variance could be formulated as a two-step mini-max optimization problem in the Stiefel manifold and the lower-dimensional HPD manifold, respectively, which was solved by the RGD algorithm. Four discriminative MIG detectors were designed in the lower-dimensional manifold with respect to the LEM distance, the AIRM distance, the JBLD and SKLD, respectively. Simulation results showed that the proposed MIG detectors could outperform their state-of-the-art counterparts and the AMF in nonhomogeneous clutter.

Potential future research includes the distributed target detection and further studies of optimization problems in Riemannian manifolds of matrices, such as the Stiefel manifold in the current study. This is certainly based on deep understanding of the geometric structures of these manifolds. Practical applications to radar or sonar via the discriminative MIG detectors should be interesting as well.

APPENDIX A PROOF OF PROPOSITION 6: THE SKLD MEAN

The SKLD mean of HPD matrices $\{\mathbf{R}_k\}_{k \in [K]}$ is the minimizer of the function

$$\begin{aligned} F(\mathbf{R}) &= \sum_{k=1}^K d_S^2(\mathbf{R}_k, \mathbf{R}) \\ &= \sum_{k=1}^K \text{tr}(\mathbf{R}_k^{-1} \mathbf{R} + \mathbf{R}^{-1} \mathbf{R}_k) - 2NK \end{aligned}$$

defined in $\mathcal{P}(N, \mathbb{C})$. Using the definition (20), gradient of the function with respect to the Frobenius metric can be obtained as

$$\nabla F(\mathbf{R}) = \sum_{k=1}^K (\mathbf{R}_k^{-1} - \mathbf{R}^{-1} \mathbf{R}_k \mathbf{R}^{-1}).$$

The stationary condition $\nabla F(\hat{\mathbf{R}}) = 0$, i.e.,

$$\sum_{k=1}^K \mathbf{R}_k^{-1} = \hat{\mathbf{R}}^{-1} \left(\sum_{k=1}^K \mathbf{R}_k \right) \hat{\mathbf{R}}^{-1},$$

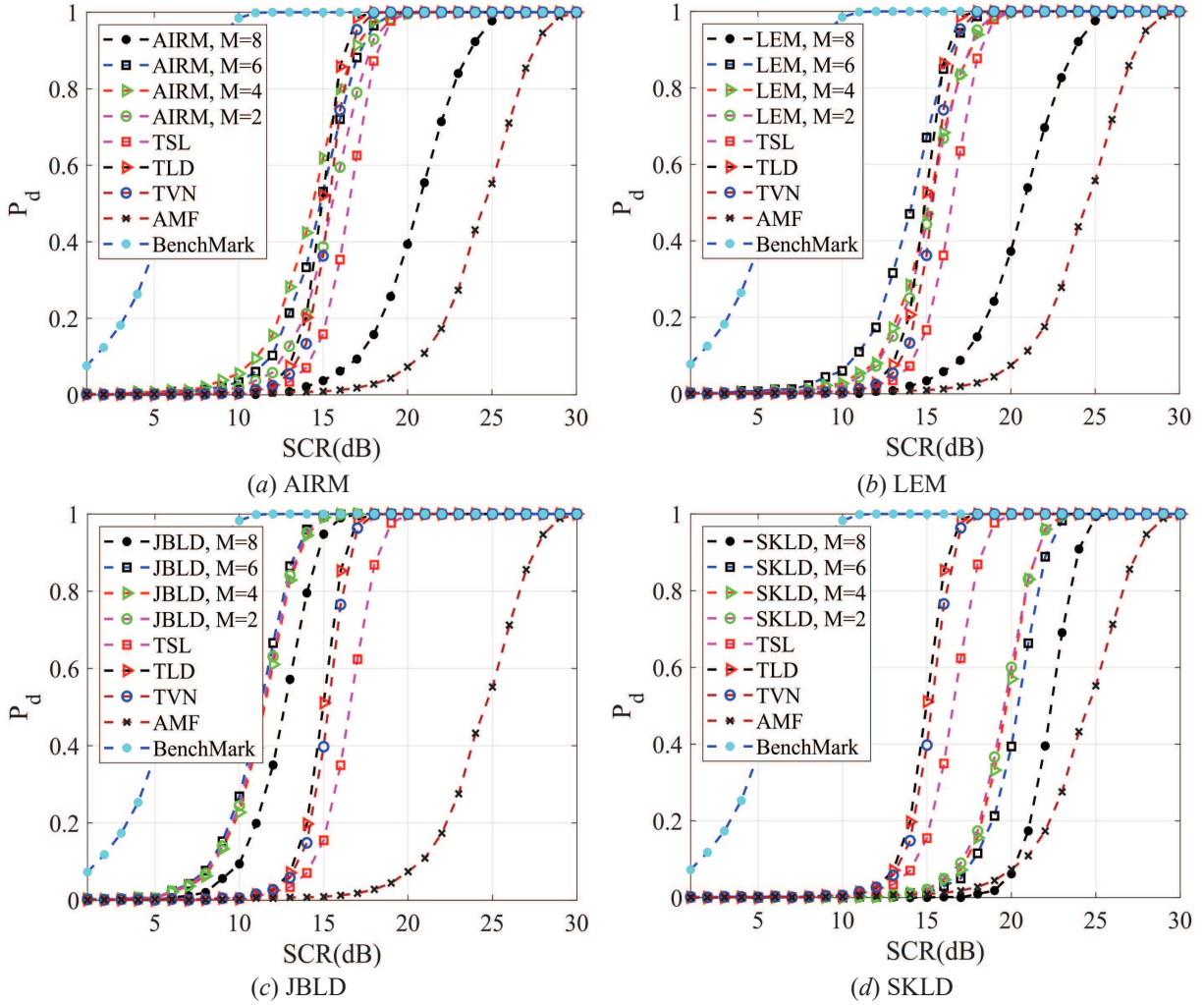


Fig. 4: The plots of P_d vs SCR for $K = 1.5M$ in the nonhomogeneous clutter with two interferences.

can be rewritten, by multiplying $\hat{\mathbf{R}}$ from the left and the right simultaneously, as

$$\hat{\mathbf{R}} \left(\sum_{k=1}^K \mathbf{R}_k^{-1} \right) \hat{\mathbf{R}} = \sum_{k=1}^K \mathbf{R}_k.$$

It is a special (continuous time) algebraic Riccati equation

$$\hat{\mathbf{R}} \mathbf{A} \hat{\mathbf{R}} = \mathbf{B}, \quad (54)$$

where $\hat{\mathbf{R}} \in \mathcal{P}(N, \mathbb{C})$ is unknown and the known coefficient matrices \mathbf{A} and \mathbf{B} are both HPD:

$$\mathbf{A} = \frac{1}{K} \sum_{k=1}^K \mathbf{R}_k^{-1}, \quad \mathbf{B} = \frac{1}{K} \sum_{k=1}^K \mathbf{R}_k. \quad (55)$$

Next we will solve the Eq. (54). Multiplying by $\mathbf{A}^{1/2}$ on both sides, we have

$$\mathbf{A}^{1/2} \hat{\mathbf{R}} \mathbf{A}^{1/2} = \mathbf{A}^{1/2} \mathbf{B} \mathbf{A}^{1/2}.$$

Noticing that its left-hand-side is exactly

$$\left(\mathbf{A}^{1/2} \hat{\mathbf{R}} \mathbf{A}^{1/2} \right)^2,$$

we obtain

$$\mathbf{A}^{1/2} \hat{\mathbf{R}} \mathbf{A}^{1/2} = \left(\mathbf{A}^{1/2} \mathbf{B} \mathbf{A}^{1/2} \right)^{1/2},$$

and hence

$$\hat{\mathbf{R}} = \mathbf{A}^{-1/2} \left(\mathbf{A}^{1/2} \mathbf{B} \mathbf{A}^{1/2} \right)^{1/2} \mathbf{A}^{-1/2},$$

where \mathbf{A} and \mathbf{B} are given by (55). This completes the proof.

APPENDIX B

PROOF OF PROPOSITION 8

At step t , the loss function with respect to the LEM reads

$$\psi(\mathbf{W}) = -\frac{1}{J+K} \sum_{i=1}^{J+K} \left\| \text{Log}(\mathbf{W}^H \mathbf{R}_i \mathbf{W}) - \text{Log} \hat{\mathbf{Z}}_t \right\|^2.$$

It suffices to show the Euclidean gradient of the function $F_i(\mathbf{W})$ with respect to the extended Frobenius metric (45), where

$$F_i(\mathbf{W}) = \left\| \text{Log}(\mathbf{W}^H \mathbf{R}_i \mathbf{W}) - \text{Log} \hat{\mathbf{Z}}_t \right\|^2.$$

Writing

$$\mathbf{A}(\varepsilon) = (\mathbf{W} + \varepsilon \mathbf{X})^H \mathbf{R}_i (\mathbf{W} + \varepsilon \mathbf{X}) \quad (56)$$

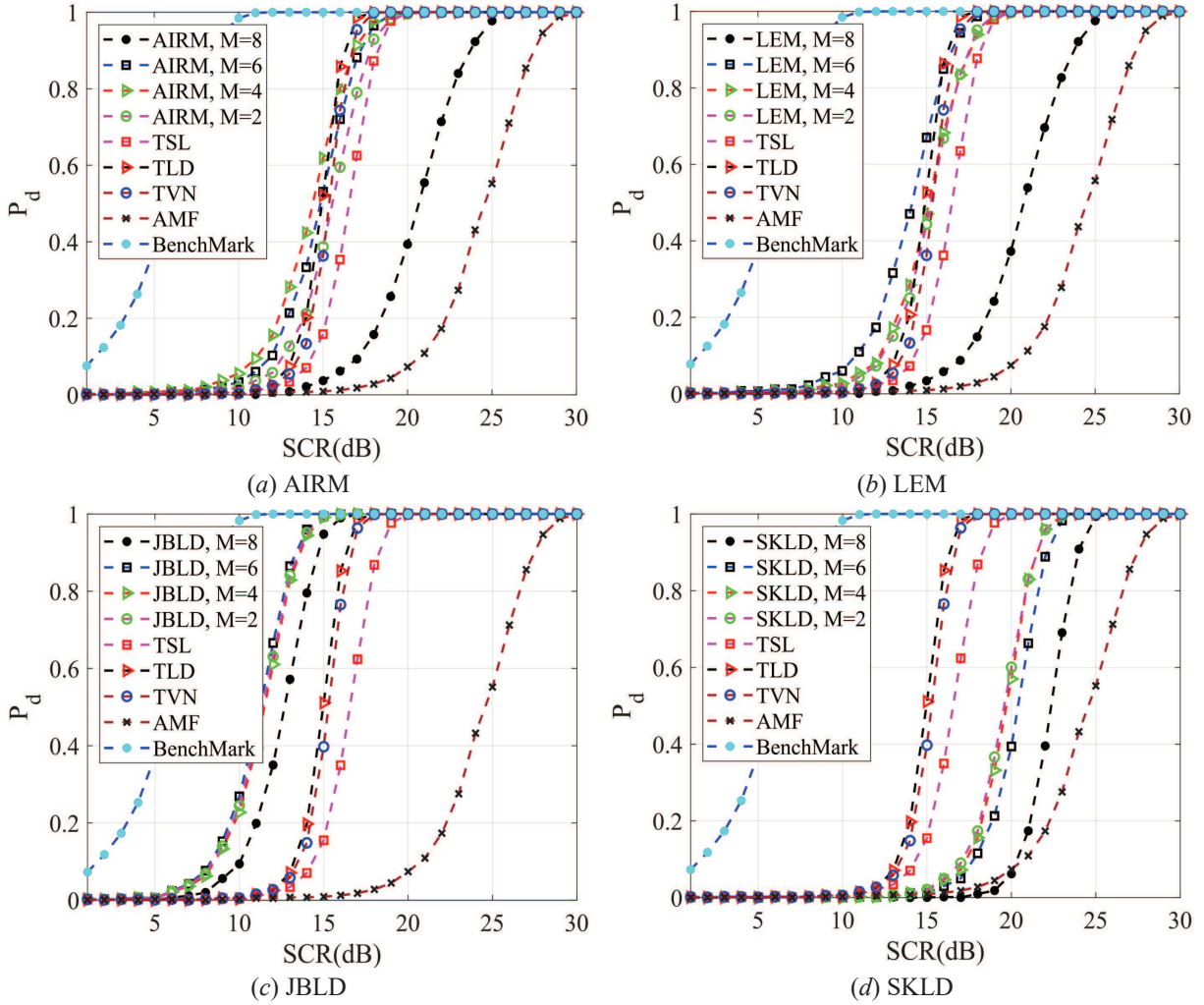


Fig. 5: The plots of P_d vs SCR for $K = 2M$ in the nonhomogeneous clutter with two interferences.

and using Eq. (20), for an $N \times M$ matrix \mathbf{X} , we have

$$\begin{aligned} \langle \nabla F_i(\mathbf{W}), \mathbf{X} \rangle &= \left. \frac{d}{d\varepsilon} \right|_{\varepsilon=0} F_i(\mathbf{W} + \varepsilon \mathbf{X}) \\ &= \left. \frac{d}{d\varepsilon} \right|_{\varepsilon=0} \text{tr} \left(\text{Log} \mathbf{A}(\varepsilon) - \text{Log} \hat{\mathbf{Z}}_t \right)^2 \\ &= 2 \text{tr} \left(\left(\text{Log} \mathbf{A}(0) - \text{Log} \hat{\mathbf{Z}}_t \right) \left. \frac{d}{d\varepsilon} \right|_{\varepsilon=0} \text{Log} \mathbf{A}(\varepsilon) \right). \end{aligned}$$

Noticing

$$\left. \frac{d}{d\varepsilon} \right|_{\varepsilon=0} \mathbf{A}(\varepsilon) = \mathbf{X}^H \mathbf{R}_i \mathbf{W} + \mathbf{W}^H \mathbf{R}_i \mathbf{X}$$

and applying Lemma 1, the above equality becomes

$$\begin{aligned} \langle \nabla F_i(\mathbf{W}), \mathbf{X} \rangle &= 4 \text{tr} \left(\left(\text{Log} \mathbf{A}(0) - \text{Log} \hat{\mathbf{Z}}_t \right) \right. \\ &\quad \times \int_0^1 [(\mathbf{A}(0) - \mathbf{I})s + \mathbf{I}]^{-1} \mathbf{W}^H \mathbf{R}_i \mathbf{X} \\ &\quad \times [(\mathbf{A}(0) - \mathbf{I})s + \mathbf{I}]^{-1} ds \Big) \\ &= 4 \text{tr} \left(\left(\mathbf{A}^{-1}(0) \text{Log} \mathbf{A}(0) - \int_0^1 [(\mathbf{A}(0) - \mathbf{I})s + \mathbf{I}]^{-1} \right. \right. \\ &\quad \times \left. \left. \left(\text{Log} \hat{\mathbf{Z}}_t \right) [(\mathbf{A}(0) - \mathbf{I})s + \mathbf{I}]^{-1} ds \right) \mathbf{W}^H \mathbf{R}_i \mathbf{X} \right). \end{aligned}$$

From the definition $\langle \nabla F_i(\mathbf{W}), \mathbf{X} \rangle = \text{tr} \left((\nabla F_i(\mathbf{W}))^H \mathbf{X} \right)$, we immediately have that

$$\begin{aligned} \nabla F_i(\mathbf{W}) &= 4 \mathbf{R}_i \mathbf{W} \left(\mathbf{A}^{-1}(0) \text{Log} \mathbf{A}(0) \right. \\ &\quad \left. - \int_0^1 [(\mathbf{A}(0) - \mathbf{I})s + \mathbf{I}]^{-1} \left(\text{Log} \hat{\mathbf{Z}}_t \right) \right. \\ &\quad \left. \times [(\mathbf{A}(0) - \mathbf{I})s + \mathbf{I}]^{-1} ds \right), \end{aligned}$$

where $\mathbf{A}(0) = \mathbf{W}^H \mathbf{R}_i \mathbf{W}$, i.e., the matrix \mathbf{V} in Proposition 8. This completes the proof.

APPENDIX C

PROOF OF PROPOSITION 10

The following lemma will be used.

Lemma 12. For any invertible matrix $\mathbf{B}(\varepsilon)$, we have

$$\frac{d}{d\varepsilon} \det \mathbf{B}(\varepsilon) = \det \mathbf{B}(\varepsilon) \text{tr} \left(\mathbf{B}^{-1}(\varepsilon) \frac{d}{d\varepsilon} \mathbf{B}(\varepsilon) \right).$$

Now the loss function can be written as

$$\psi(\mathbf{W}) = -\frac{1}{J+K} \sum_{i=1}^{J+K} F_i(\mathbf{W})$$

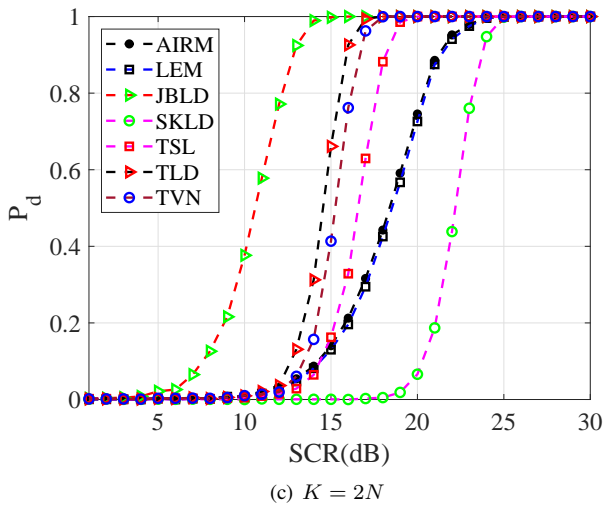
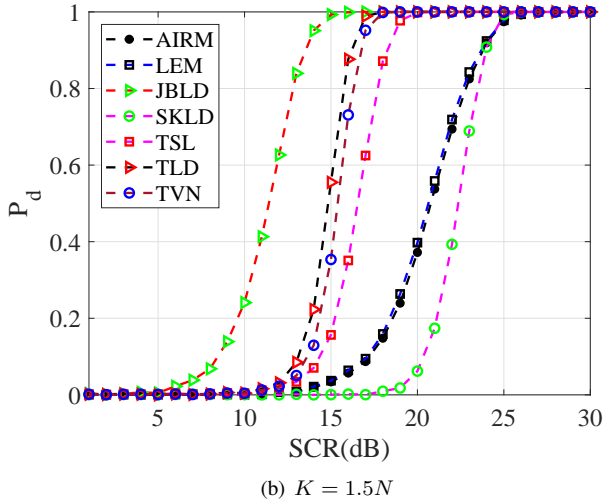
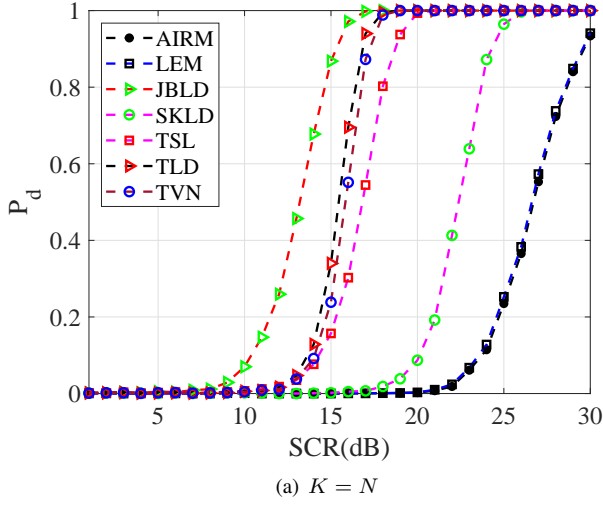


Fig. 6: P_d vs SCR for different measures

with

$$F_i(\mathbf{W}) = \ln \det \left(\frac{\mathbf{A}(0) + \hat{\mathbf{Z}}_t}{2} \right) - \frac{1}{2} \ln \det \left(\mathbf{A}(0) \hat{\mathbf{Z}}_t \right),$$

where $\mathbf{A}(\varepsilon)$ is given by Eq. (56) and $\mathbf{A}(0) = \mathbf{W}^H \mathbf{R}_i \mathbf{W}$. Using Lemma 12, definition of the Euclidean gradient gives

$$\begin{aligned} \langle \nabla F_i(\mathbf{W}), \mathbf{X} \rangle &= \left. \frac{d}{d\varepsilon} \right|_{\varepsilon=0} \ln \det \left(\frac{\mathbf{A}(\varepsilon) + \hat{\mathbf{Z}}_t}{2} \right) \\ &\quad - \frac{1}{2} \left. \frac{d}{d\varepsilon} \right|_{\varepsilon=0} \ln \det \left(\mathbf{A}(\varepsilon) \hat{\mathbf{Z}}_t \right) \\ &= \text{tr} \left(\left(2 \left(\mathbf{A}(0) + \hat{\mathbf{Z}}_t \right)^{-1} - \mathbf{A}^{-1}(0) \right) \mathbf{W}^H \mathbf{R}_i \mathbf{X} \right). \end{aligned}$$

Consequently, we have

$$\nabla F_i(\mathbf{W}) = \mathbf{R}_i \mathbf{W} \left(2 \left(\mathbf{A}(0) + \hat{\mathbf{Z}}_t \right)^{-1} - \mathbf{A}^{-1}(0) \right)$$

and

$$\nabla \psi(\mathbf{W}) = -\frac{1}{J+K} \sum_{i=1}^{J+K} \nabla F_i(\mathbf{W}),$$

that finishes the proof.

APPENDIX D PROOF OF PROPOSITION 11

Similarly, we write the loss function as

$$\psi(\mathbf{W}) = -\frac{1}{J+K} \sum_{i=1}^{J+K} F_i(\mathbf{W}),$$

where

$$\begin{aligned} F_i(\mathbf{W}) &= \frac{1}{2} \text{tr} \left(\left(\mathbf{W}^H \mathbf{R}_i \mathbf{W} \right)^{-1} \hat{\mathbf{Z}}_t \right. \\ &\quad \left. + \hat{\mathbf{Z}}_t^{-1} \left(\mathbf{W}^H \mathbf{R}_i \mathbf{W} \right) - 2\mathbf{I} \right). \end{aligned}$$

Euclidean gradient of the function $F_i(\mathbf{W})$ is given by

$$\begin{aligned} \langle \nabla F_i(\mathbf{W}), \mathbf{X} \rangle &= \left. \frac{1}{2} \frac{d}{d\varepsilon} \right|_{\varepsilon=0} \text{tr} \left(\mathbf{A}^{-1}(\varepsilon) \hat{\mathbf{Z}}_t + \hat{\mathbf{Z}}_t^{-1} \mathbf{A}(\varepsilon) \right) \\ &= \frac{1}{2} \text{tr} \left(\left(\hat{\mathbf{Z}}_t^{-1} - \mathbf{A}^{-1}(0) \hat{\mathbf{Z}}_t^{-1} \mathbf{A}^{-1}(0) \right) \right. \\ &\quad \left. \times \left(\mathbf{X}^H \mathbf{R}_i \mathbf{W} + \mathbf{W}^H \mathbf{R}_i \mathbf{X} \right) \right) \\ &= \text{tr} \left(\left(\hat{\mathbf{Z}}_t^{-1} - \mathbf{A}^{-1}(0) \hat{\mathbf{Z}}_t \mathbf{A}^{-1}(0) \right) \mathbf{W}^H \mathbf{R}_i \mathbf{X} \right), \end{aligned}$$

and consequently, we obtain

$$\nabla F_i(\mathbf{W}) = \mathbf{R}_i \mathbf{W} \left(\hat{\mathbf{Z}}_t^{-1} - \mathbf{A}^{-1}(0) \hat{\mathbf{Z}}_t \mathbf{A}^{-1}(0) \right).$$

Here, $\mathbf{A}(\varepsilon)$ is given by (56) and $\mathbf{A}(0) = \mathbf{W}^H \mathbf{R}_i \mathbf{W}$. This completes the proof.

REFERENCES

- [1] O. Besson and D. Orlando, "Adaptive detection in nonhomogeneous environments using the generalized eigenrelation," *IEEE Signal Processing Letters*, vol. 14, no. 10, pp. 731–734, Oct 2007.
- [2] P. Wang, H. Li, and B. Himed, "Moving target detection using distributed MIMO radar in clutter with nonhomogeneous power," *IEEE Transactions on Signal Processing*, vol. 59, no. 10, pp. 4809–4820, 2011.
- [3] D. Ciunzo, D. Orlando, and L. Pallotta, "On the maximal invariant statistic for adaptive radar detection in partially homogeneous disturbance with persymmetric covariance," *IEEE Signal Processing Letters*, vol. 23, no. 12, pp. 1830–1834, 2016.
- [4] D. Ciunzo, A. De Maio, and D. Orlando, "A unifying framework for adaptive radar detection in homogeneous plus structured interference—part II: Detectors design," *IEEE Transactions on Signal Processing*, vol. 64, no. 11, pp. 2907–2919, 2016.
- [5] Y. Rong, A. Aubry, A. De Maio, and M. Tang, "Adaptive radar detection in Gaussian interference using clutter-free training data," *IEEE Transactions on Signal Processing*, vol. 70, pp. 978–993, 2022.
- [6] D. Lee, J. Shin, D. Do, S. Choi, and H. Kim, "Robust LFM target detection in wideband sonar systems," *IEEE Transactions on Aerospace and Electronic Systems*, vol. 53, no. 5, pp. 2399–2412, 2017.
- [7] I. Bekkerman and J. Tabrikian, "Target detection and localization using MIMO radars and sonars," *IEEE Transactions on Signal Processing*, vol. 54, no. 10, pp. 3873–3883, 2006.
- [8] K. M. Wong, J. Zhang, J. Liang, and H. Jiang, "Mean and median of PSD matrices on a Riemannian manifold: Application to detection of narrow-band sonar signals," *IEEE Transactions on Signal Processing*, vol. 65, no. 24, pp. 6536–6550, 2017.
- [9] Y. Fang, A. Noel, N. Yang, A. W. Eckford, and R. A. Kennedy, "Symbol-by-symbol maximum likelihood detection for cooperative molecular communication," *IEEE Transactions on Communications*, vol. 67, no. 7, pp. 4885–4899, 2019.
- [10] A. Aubry, A. De Maio, L. Pallotta, and A. Farina, "Maximum likelihood estimation of a structured covariance matrix with a condition number constraint," *IEEE Transactions on Signal Processing*, vol. 60, no. 6, pp. 3004–3021, 2012.
- [11] P. Wang, H. Li, and B. Himed, "Knowledge-aided parametric tests for multichannel adaptive signal detection," *IEEE Transactions on Signal Processing*, vol. 59, no. 12, pp. 5970–5982, 2011.
- [12] A. De Maio, D. Orlando, C. Hao, and G. Foglia, "Adaptive detection of point-like targets in spectrally symmetric interference," *IEEE Transactions on Signal Processing*, vol. 64, no. 12, pp. 3207–3220, 2016.
- [13] F. Bandiera, O. Besson, and G. Ricci, "Knowledge-aided covariance matrix estimation and adaptive detection in compound-Gaussian noise," *IEEE Transactions on Signal Processing*, vol. 58, no. 10, pp. 5391–5396, Oct 2010.
- [14] E. Conte, A. De Maio, A. Farina, and G. Foglia, "Design and analysis of a knowledge-aided radar detector for Doppler processing," *IEEE Transactions on Aerospace and Electronic Systems*, vol. 42, no. 3, pp. 1058–1079, 2006.
- [15] A. D. Maio, S. D. Nicola, L. Landi, and A. Farina, "Knowledge-aided covariance matrix estimation: a MAXDET approach," *IET Radar, Sonar & Navigation*, vol. 3, no. 4, pp. 341–356, 2009.
- [16] A. D. Maio, A. Farina, and G. Foglia, "Design and experimental validation of knowledge-based constant false alarm rate detectors," *IET Radar, Sonar & Navigation*, vol. 1, no. 4, pp. 308–316, Aug 2007.
- [17] A. De Maio, A. Farina, and G. Foglia, "Knowledge-aided Bayesian radar detectors & their application to live data," *IEEE Transactions on Aerospace and Electronic Systems*, vol. 46, no. 1, pp. 170–183, Jan 2010.
- [18] D. Ciunzo, A. De Maio, and D. Orlando, "On the statistical invariance for adaptive radar detection in partially homogeneous disturbance plus structured interference," *IEEE Transactions on Signal Processing*, vol. 65, no. 5, pp. 1222–1234, 2017.
- [19] C. R. Rao, *Information and the Accuracy Attainable in the Estimation of Statistical Parameters*. New York: Springer, 1992, pp. 235–247.
- [20] N. N. Chentsov, *Statistical Decision Rules and Optimal Inference*. Moscow: Nauka, 1972, in Russian.
- [21] B. Efron, "Defining the curvature of a statistical problem (with applications to second order efficiency)," *Annals of Statistics*, vol. 3, no. 6, pp. 1189–1242, 1975.
- [22] S. Amari, "Information geometry and the EM algorithm," in *ICANN '94*, M. Marinaro and P. G. Morasso, Eds. London: Springer, 1994, pp. 675–680.
- [23] L. Peng, H. Sun, D. Sun, and J. Yi, "The geometric structures and instability of entropic dynamical models," *Advances in Mathematics*, vol. 227, no. 1, pp. 459–471, 2011.
- [24] T. Li, L. Peng, and H. Sun, "The geometric structure of the inverse gamma distribution," *Contributions to Algebra and Geometry*, vol. 49, no. 1, pp. 217–225, 2008.
- [25] S.-i. Amari and H. Nagaoka, *Methods of Information Geometry*. AMS, 2000, vol. 191.
- [26] H. Sun, Z. Zhang, L. Peng, and X. Duan, *An Elementary Introduction to Information Geometry*. Beijing: Science Press, 2016.
- [27] B. Balaji, F. Barbaresco, and A. Decurninge, "Information geometry and estimation of Toeplitz covariance matrices," in *2014 International Radar Conference*, 2014, pp. 1–4.
- [28] M. Coutino, R. Pribic, and G. Leus, "Direction of arrival estimation based on information geometry," in *2016 IEEE International Conference on Acoustics, Speech and Signal Processing (ICASSP)*, 2016, pp. 3066–3070.
- [29] A. Aubry, A. D. Maio, L. Pallotta, and A. Farina, "Covariance matrix estimation via geometric barycenters and its application to radar training data selection," *IET Radar, Sonar & Navigation*, vol. 7, no. 6, pp. 600–614, July 2013.
- [30] J. Lapuyade-Lahorgue and F. Barbaresco, "Radar detection using siegel distance between autoregressive processes, application to HF and X-band radar," in *2008 IEEE Radar Conference*, May 2008, pp. 1–6.
- [31] X. Hua, Y. Cheng, H. Wang, Y. Qin, and Y. Li, "Geometric means and medians with applications to target detection," *IET Signal Processing*, vol. 11, no. 6, pp. 711–720, 2017.
- [32] X. Hua and L. Peng, "MIG median detectors with manifold filter," *Signal Processing*, vol. 188, p. 108176, 2021.
- [33] M. Ruiz and F. Barbaresco, "Radar detection for non-stationary Doppler signal in one burst based on information geometry distance between paths," in *2015 16th International Radar Symposium (IRS)*, June 2015, pp. 422–427.
- [34] M. Arnaudon, F. Barbaresco, and L. Yang, "Riemannian medians and means with applications to radar signal processing," *IEEE Journal of Selected Topics in Signal Processing*, vol. 7, no. 4, pp. 595–604, Aug 2013.
- [35] F. Barbaresco, "Innovative tools for radar signal processing based on Cartan's geometry of SPD matrices information geometry," in *2008 IEEE Radar Conference*, May 2008, pp. 1–6.
- [36] Z. Liu and F. Barbaresco, *Doppler information geometry for wake turbulence monitoring*. Berlin, Heidelberg: Springer Berlin Heidelberg, 2013, pp. 277–290.
- [37] F. Barbaresco and U. Meier, "Radar monitoring of a wake vortex: Electromagnetic reflection of wake turbulence in clear air," *Comptes Rendus Physique*, vol. 11, no. 1, pp. 54–67, 2010, propagation and remote sensing.
- [38] F. Barbaresco, "Coding statistical characterization of radar signal fluctuation for Lie group machine learning," in *2019 International Radar Conference (RADAR)*, 2019, pp. 1–6.
- [39] B. Balaji and F. Barbaresco, "Application of Riemannian mean of covariance matrices to space-time adaptive processing," in *2012 9th European Radar Conference*, 2012, pp. 50–53.
- [40] A. Decurninge and F. Barbaresco, "Robust Burg estimation of radar scatter matrix for autoregressive structured SIRV based on fréchet medians," *IET Radar, Sonar & Navigation*, vol. 11, no. 1, pp. 78–89, 2017.
- [41] X. Hua, Y. Cheng, H. Wang, Y. Qin, Y. Li, and W. Zhang, "Matrix CFAR detectors based on symmetrized Kullback–Leibler and total Kullback–Leibler divergences," *Digital Signal Processing*, vol. 69, pp. 106–116, 2017.
- [42] X. Hua, Y. Cheng, H. Wang, Y. Qin, and D. Chen, "Geometric target detection based on total Bregman divergence," *Digital Signal Processing*, vol. 75, pp. 232–241, 2018.
- [43] X. Hua, Y. Ono, L. Peng, Y. Cheng, and H. Wang, "Target detection within nonhomogeneous clutter via total Bregman divergence-based matrix information geometry detectors," *IEEE Transactions on Signal Processing*, vol. 69, pp. 4326–4340, 2021.
- [44] A. De Maio, L. Pallotta, J. Li, and P. Stoica, "Loading factor estimation under affine constraints on the covariance eigenvalues with application to radar target detection," *IEEE Transactions on Aerospace and Electronic Systems*, vol. 55, no. 3, pp. 1269–1283, 2019.
- [45] A. Aubry, A. De Maio, and L. Pallotta, "A geometric approach to covariance matrix estimation and its applications to radar problems," *IEEE Transactions on Signal Processing*, vol. 66, no. 4, pp. 907–922, 2018.
- [46] J. Liu, W. Liu, Y. Gao, S. Zhou, and X. Xia, "Persymmetric adaptive detection of subspace signals: Algorithms and performance analysis," *IEEE Transactions on Signal Processing*, vol. 66, no. 23, pp. 6124–6136, 2018.

- [47] Y. I. Abramovich, N. K. Spencer, and A. Y. Gorokhov, "Modified GLRT and AMF framework for adaptive detectors," *IEEE Transactions on Aerospace and Electronic Systems*, vol. 43, no. 3, pp. 1017–1051, 2007.
- [48] B. D. Carlson, "Covariance matrix estimation errors and diagonal loading in adaptive arrays," *IEEE Transactions on Aerospace and Electronic Systems*, vol. 24, no. 4, pp. 397–401, 1988.
- [49] L. Du, J. Li, and P. Stoica, "Fully automatic computation of diagonal loading levels for robust adaptive beamforming," *IEEE Transactions on Aerospace and Electronic Systems*, vol. 46, no. 1, pp. 449–458, 2010.
- [50] M. R. Bridson and A. Häfliger, *Metric Spaces of Non-Positive Curvature*. Springer Science & Business Media, 2013, vol. 319.
- [51] O. Yair, M. Ben-Chen, and R. Talmon, "Parallel Transport on the Cone Manifold of SPD Matrices for Domain Adaptation," *IEEE Transactions on Signal Processing*, vol. 67, no. 7, pp. 1797–1811, 2019.
- [52] G. Luo, J. Wei, W. Hu, and S. J. Maybank, "Tangent fisher vector on matrix manifolds for action recognition," *IEEE Transactions on Image Processing*, vol. 29, pp. 3052–3064, 2020.
- [53] N. J. Higham, *Functions of Matrices: Theory and Computation*. Philadelphia: SIAM, 2008.
- [54] M. Moakher, "A differential geometric approach to the geometric mean of symmetric positive-definite matrices," *SIAM Journal on Matrix Analysis and Applications*, vol. 26, no. 3, pp. 735–747, 2005.
- [55] V. Arsigny, P. Fillard, X. Pennec, and N. Ayache, "Geometric means in a novel vector space structure on symmetric positive definite matrices," *SIAM Journal on Matrix Analysis and Applications*, vol. 29, no. 1, pp. 328–347, 2007.
- [56] A. Cherian, S. Sra, A. Banerjee, and N. Papanikolopoulos, "Jensen–Bregman LogDet divergence with application to efficient similarity search for covariance matrices," *IEEE Transactions on Pattern Analysis and Machine Intelligence*, vol. 35, no. 9, pp. 2161–2174, 2013.
- [57] M. Charfi, Z. Chebbi, M. Moakher, and B. C. Vemuri, "Using the Bhattacharyya mean for the filtering and clustering of positive definite matrices," in *Geometric Science of Information*, F. Nielsen and F. Barbaresco, Eds. Berlin, Heidelberg: Springer Berlin Heidelberg, 2013, pp. 551–558.
- [58] M. Moakher, "On the averaging of symmetric positive-definite tensors," *Journal of Elasticity volume*, vol. 82, pp. 273–296, 2006.
- [59] X. Hua, L. Peng, W. Liu, Y. Cheng, and H. Sun, "Supervised manifold projection-based MIG detectors in nonhomogeneous clutter," 2021, preprint.
- [60] S. Said, L. Bombrun, Y. Berthoumieu, and J. H. Manton, "Riemannian Gaussian distributions on the space of symmetric positive definite matrices," *IEEE Transactions on Information Theory*, vol. 63, no. 4, pp. 2153–2170, 2017.
- [61] S. T. Smith, *Geometric Optimization Methods for Adaptive Filtering*. Cambridge, Massachusetts: PhD Thesis, Harvard University, 1993.
- [62] C. Udriște, *Convex Functions and Optimization Methods on Riemannian Manifolds*. Dordrecht: Springer Science+Business Media, B.V., 1994.
- [63] P.-A. Absil, R. Mahony, and R. Sepulchre, *Optimization Algorithms on Matrix Manifolds*. Princeton, NJ: Princeton University Press, 2008.
- [64] E. J. Kelly, "An adaptive detection algorithm," *IEEE Transactions on Aerospace and Electronic Systems*, vol. AES-22, no. 2, pp. 115–127, March 1986.